Research Square

Preprints are preliminary reports that have not undergone peer review.
They should not be considered conclusive, used to inform clinical practice,
or referenced by the media as validated information.

Experimental Study of Mixed Convection and Thermal Radiation Heat Transfer in Horizontal Rectangular Ducts with Different Heating Orientations

ADHAVAN VINAYAGAMOORTHY
SASTRA University
Rajamohan Ganesan
rajamohan@mech.sastra.ac.in

SASTRA University

Research Article

Keywords: Experimental investigation, Heat transfer, Mixed convection, Radiation, Rectangular duct, Heating orientation, Nusselt number, Reynolds number

Posted Date: November 9th, 2026

DOI: https://doi.org/10.21203/rs.3.rs-11045452/v1

License: This work is licensed under a Creative Commons Attribution 4.0 International License.
Read Full License

Additional Declarations: No competing interests reported.

Experimental Study of Mixed Convection and Thermal Radiation Heat Transfer in Horizontal Rectangular Ducts with Different Heating Orientations

Adhavan Vinayagamoorthy. Rajamohan Ganesan*

School of Mechanical Engineering, SASTRA Deemed University, Thanjavur, Tamil Nadu, India

*Corresponding author: rajamohan@mech.sastra.ac.in

Abstract

The current experimental work examines the combined effects of mixed convection and surface radiation on heating a horizontal rectangular duct from three distinct bottom orientations: CS1 (bottom), CS2 (top), and CS3 (side). The rectangular duct section consists of one heated isothermal wall, and the remaining walls are maintained under adiabatic conditions. The effects of Reynolds number, heat flow, surface emissivity, and heating orientation on the heated-wall temperature and total Nusselt number for convective and radiative heat transfer were systematically assessed. The findings show that forced-convection effects are strengthened as the Reynolds number increases from 978 to 1956, thereby significantly lowering the heated-wall temperature. The wall temperature increases, and the convective Nusselt number decreases by 5–13% as the applied heat flux increases from 644 to 1659 W/m². Among the three heating orientations, CS1 demonstrates the highest heat-transfer performance, followed by CS2 and CS3, respectively. Increasing the surface emissivity from 0.05 to 0.85 reduces the average wall temperature by approximately 15–16% and enhances the convective Nusselt number by 21–35%. The radiative Nusselt number rises significantly, indicating that surface radiation plays a major role in the total heat-transfer process. Stable thermal behaviour along the duct is shown by the axial profiles of the heat-transfer parameters being comparatively uniform. Overall, the results show that bottom heating (CS1) in conjunction with a high-emissivity surface offers the best heat-transfer performance and can be used successfully for heat dissipation and passive thermal management applications.

Keywords: Experimental investigation, Heat transfer, Mixed convection, Radiation, Rectangular duct, Heating orientation, Nusselt number, Reynolds number.

Abbreviations

List of symbols		
A_s	Heated wall surface Area	[m²]
D_h	Hydraulic diameter for the rectangular test section	[m]
H	Height of the rectangular test section	[m]
h_c	Convective heat transfer coefficient	[W/m^2·K]
h_r	Radiative heat transfer coefficient	[W/m²·K]
I	current	A (ampere)
k	Thermal conductivity of air	[W/m K]
L	Length of the rectangular duct section	[m]
Nu_t	Total Nusselt number	-
Nu_c	Convective Nusselt number	-
Nu_r	Radiation Nusselt number	-
Q_t	Total heat transfer	[W]
Q_c	Convective heat transfer	[W]
Q_r	Radiation heat transfer	[W]
q	Heated wall surface heat flux	W/m^2
T_b	Bulk mean air temperature	[K]
T_{in}	Entry air temperature to the duct section	[K]
T_{out}	Exit air temperature from the duct section	[K]
T_w	Heated wall surface temperature	[K]
V	Voltage	V (volt)
W	Width of the rectangular test section	[m]
z	Distance from the inlet to the exit of the duct	[m]
Z/D_h	Dimensionless distance	-
Greek symbols		

ε	Emissivity of the wall surface	-
σ	Stefan–Boltzmann constant (5.67×10^{-8})	W/m^2K^4
Subscript		
s	Surface	
c	Convection	
r	Radiation	

Introduction

Rectangular ducts are commonly used in thermal engineering systems for effective heat transmission, including solar collectors, electronic cooling devices, and heat exchangers. The combined effects of controlled and natural convection, heating orientation, and surface radiation greatly influence thermal performance. However, there hasn't been much focus on radiation consequences in horizontal square ducts. Thus, across various heating orientations, the current study examines combined convective and radiative heat transfer. The literature shows that surface radiation has been completely ignored in most mixed-convection investigations in ducts, particularly for various wall-heating orientations. With a focus on heating configuration and surface emissivity and their impact on total heat transfer, the current work examines the combined impacts of mixed convection and radiation for differentially heated walls.

The study experimentally investigated laminar mixed convection in a horizontal rectangular duct, with the lower, upper, and both surfaces subjected to constant heat flux. The results showed that buoyancy-induced secondary flow significantly enhanced heat transfer, particularly along the lower heated surface. At high heat flux and low Reynolds number, heat-transfer enhancement reached nearly 98% compared with pure forced convection [1]. Wavy delta winglets significantly enhance heat transfer in solar air heater ducts. Despite greater friction losses, the ideal arrangement produced a maximum thermo-hydraulic performance of 2.08 and a Nusselt number 2.23 times higher at Re = 5000 [2]. Heat transfer is improved by raising the Reynolds and Grashof numbers on laminar mixed convection in finned channels. At higher longitudinal orientations, increasing the orientation angle can improve the average heat-transfer coefficient and fin efficacy by up to 25% by strengthening buoyancy-induced secondary flow [3]. The semitransparent partitions had a major impact on temperature distribution and natural convection flow. The enclosure temperature is raised, and heat loss via radiation through these walls is decreased. However, thermal conductivity primarily affects wall temperature at lower levels, and wall transmittance significantly impacts thermal performance [4].

The study experimentally examined both vertical and horizontal orientations while accounting for wall emissivity and Reynolds number. The results showed that, whereas surface emissivity significantly affected radiation and the total Nusselt number, vertical channels enhanced heat

transfer due to buoyancy effects [5]. The Reynolds number, wall emissivity, temperature differential, and heat flux significantly influence heat transfer. The combined effects of convection, radiation, and buoyancy are demonstrated by higher Reynolds numbers, which improve convective heat transfer, and higher emissivity, which improves radiative heat transfer [6]. The overall Nusselt number is strongly influenced by the Reynolds number, wall emissivity, and heater position, according to the results. Black surfaces increased radiation, and bottom heating offered better heat dissipation. Overall heat transmission was significantly influenced by surface radiation, especially at lower Reynolds numbers [7].

Experimental results demonstrated that bottom-wall heating significantly modifies flow structure in horizontal square channels. Strong buoyancy generated secondary circulation, turbulence, and complex three-dimensional flow, with backflow occurring at high Gr/Re^2. Proper orthogonal decomposition analysis identified dominant convective cells near the heated wall [8]. By increasing buoyancy-driven secondary flow and thermal instability, increasing inclination disturbs the thermal boundary layer and enhances heat transfer. The transverse Richardson and Rayleigh numbers accurately describe the mixed-convection behaviour in inclined rectangular channels; higher Reynolds numbers postpone instability [9]. Mixed convection in vertical rectangular ducts is significantly influenced by solar-induced volumetric heating. By increasing the aspect ratio, lateral-wall effects are lessened, and parallel-channel behaviour is approached. In mixed-convection situations, solar radiation may cause flow reversal and alter temperature, velocity, friction factor, and Nusselt number [10]. Eccentricity has a substantial impact on local convective heat transport in annular ducts, as established experimentally. The heat transfer coefficient reached its maximum at the biggest annular gap and rose with Reynolds number. Compared to concentric ducts, eccentric layouts improved heat transmission [11]. Surface roughness considerably improved in combined convection in rectangular microchannels, according to experimental results. Because of improved mixing and boundary-layer interactions, higher roughness raised the Nusselt number, especially at lower hydraulic diameters. Forced convection was more severely impacted by roughness than natural convection [12]. Non-uniform microchannels enhance fluid mixing and heat transfer by generating secondary flows that disrupt thermal boundary layers. The optimum thermohydraulic performance is achieved with topology-optimised channels, which balance pressure-drop penalties and deliver 50–80% heat-transfer enhancement and Performance evaluation criterion values of 1.6–2.3 [13].

According to the study, turbulent mixed convection in 2x2 subchannels is greatly influenced by buoyancy. While downstream heat-transfer enhancement increased, increasing the buoyancy parameter disrupted velocity profiles, inhibited heat transfer, altered secondary-flow structures, and reduced spacer-grid enhancement near the exit [14]. The experimental study has shown that the Heater position significantly affects mixed-convection heat transfer. While downstream heaters warmed up, the heater closest to the intake showed the lowest temperature. The Nusselt number increased quickly at low Richardson values and was highly dependent on the Reynolds number. The efficacy of thermal management was enhanced by optimally placing heaters [15]. Parametric and comparative studies show that radiation significantly increases heat dissipation from discrete heaters, reducing peak plate temperature by approximately 5% under forced convection and 35% under free convection. Compared to discrete heating setups, uniform heating resulted in more consistent temperature distributions and lower peak temperatures [16]. The enclosure geometry, aspect ratio, base angle, baffles, Rayleigh number, and Prandtl number significantly influence flow and temperature

distributions. The authors concluded that modifying enclosure geometry offers considerable potential for enhancing natural convection heat transfer performance [17].

Increasing heater clearance improves mixed-convection cooling by increasing global conductance by 20.84% and reducing hot-spot temperature by up to 10.77%. Low Reynolds numbers, radiation is significant, but as the flow rate rises, convection takes over, with clearance having a major impact on radiative heat transfer [18]. Increasing the Reynolds number and surface emissivity improves heat transport and significantly reduces the maximum cavity temperature. Stronger forced convection and heat radiation, in turn, enhance the overall thermal performance of the ventilated horizontal channel [19]. A comprehensive review emphasises that the Prandtl number, the shape of the test section, and positioning significantly affect combined convective heat transfer. There is minimal research on middle Prandtl-number fluids, with circular horizontal tubes predominating. Heat transfer is improved via passive methods and nanofluids, suggesting substantial promise for enhanced energy applications and thermal storage [20]. The numerical investigation shows that coupled natural convection–radiation heat transport is significantly influenced by plate orientation. While vertical plates reduced fluctuation, horizontal plates generated the greatest Nusselt-number variation and significant vortex stretching. The behaviour of tilted plates was intermediate, indicating that orientation significantly affects local heat transfer and flow separation [21].

Flow-directing fins and triangular barriers improve mixed-convection heat transfer. The Al2O3–water nanofluid enhanced thermal performance; the 60° triple-obstacle configuration achieved an 8.87% improvement in the performance evaluation criteria and a 12.76% higher Nusselt number than the comparable quadruple configuration [22]. Honeycomb, radial, and flaring heat sinks under forced convection were compared experimentally. With a much reduced thermal resistance and the maximum heat transfer coefficient and Nusselt number, the honeycomb heat sink demonstrated excellent heat dissipation performance for electronic cooling applications [23]. Experimental research was done on mixed convection in a chamber with a reciprocating top surface and a heated lower wall. An analysis was conducted to determine how flow and heat transmission were affected by the Richardson number, aspect ratio, and dimensionless period. With an improved Nusselt number at a lower Richardson number and a larger aspect ratio, the results demonstrated strong experimental–numerical agreement [24]. Increasing the Reynolds number improves convective heat transfer, according to computational and experimental studies of mixed convection with surface radiation in vented enclosures. Radiation significantly improves thermal performance as emissivity and aspect ratio increase, while higher emissivity reduces the maximum and average heated-surface temperatures [25].

According to the reviewed literature, the Reynolds number, Grashof number, Richardson number, heating arrangement, geometry, and surface characteristics all significantly affect convection heat transfer in channels. Buoyancy-induced secondary flow can enhance heat transfer, especially for bottom heating and low Reynolds numbers, according to prior research. Heat transfer is improved by several passive enhancement techniques, including fins, winglets, roughness, obstructions, and altered channel geometry, although these often come at the expense of higher pressure drops. The importance of thermal radiation has been the subject of several studies, which have shown that surface emissivity significantly influences radiative and total heat transfer, especially at low flow rates when natural convection predominates. However, most research focuses on isolated radiation scenarios, and there is a dearth of

experimental data on the effects of surface emissivity and differential wall heating in horizontal rectangular ducts. The combined effects of mixed convection and wall-surface thermal radiation on thermal performance are experimentally examined under different orientations to close this research gap.

Experimental Investigation

Experimental methods

In a horizontal rectangular duct heated from three distinct directions, the combined impact of mixed convection and thermal radiation from the wall surface on heat transfer was examined experimentally. Figures 1 and 2 show the schematic and photograph of the experimental test rig. The positions of the heated and adiabatic walls, as well as the general geometric structure, are depicted in Figure 3, a cross-sectional image of the test section. The overall test section consisted of a horizontal rectangular test duct; one heated isothermal wall; the remaining walls maintained under adiabatic conditions; a blower with a flow-control arrangement; a heater with a variable transformer; a data logger; thermocouples; and an anemometer.

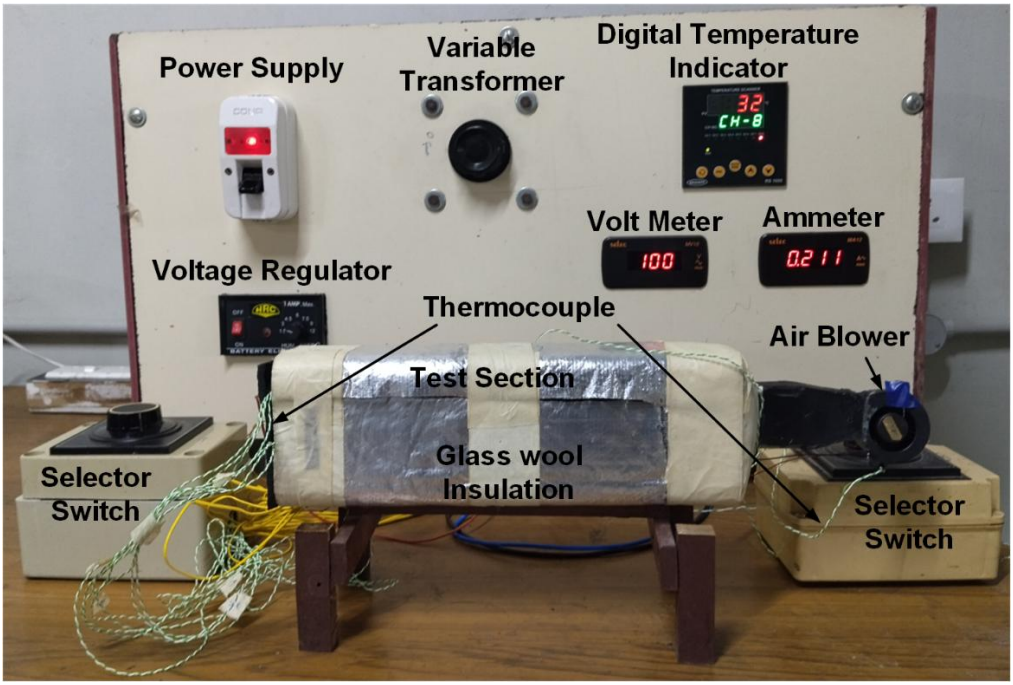


Fig. 1 Picture of the experimental test apparatus

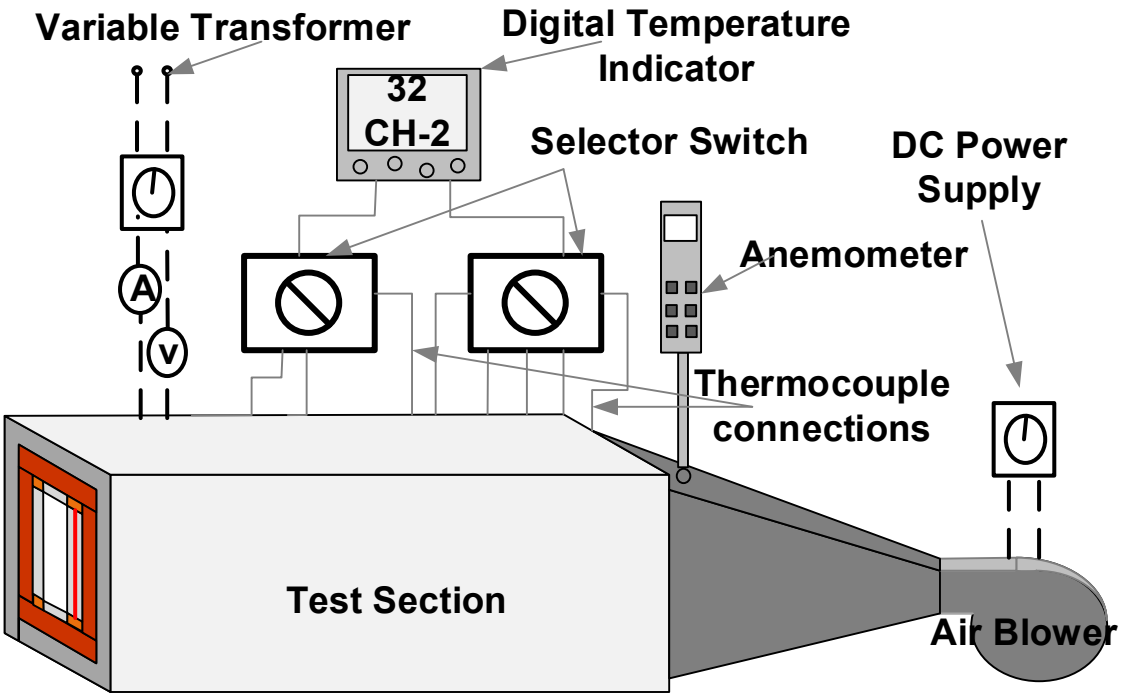


Fig. 2 Schematic illustration of the apparatus

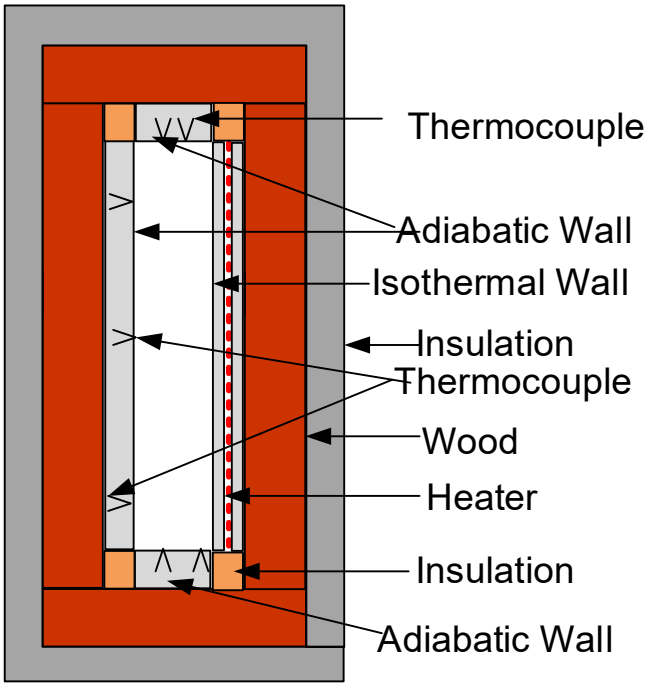


Fig. 3 Sectional view of the testing device

The test duct had internal dimensions of 300 mm (length) × 40 mm (width) × 11 mm (height). The heated wall surface area of the duct comprised a rectangular aluminium plate measuring 300 mm in length × 40 mm in width, matching the full length and width of the duct cross-

section. A silicon rubber heater was mounted within the heated wall to provide the duct wall with a consistent heat flux. A variable transformer was used to power the heater and control the amount of heat it delivered. A digital voltmeter and an ammeter were used to measure the voltage and current, respectively, to determine the electric power supplied to the heater. The heated plate assembly was mounted to the test section by the bottom wall, one side wall, or the top wall, allowing the same test section to be reconfigured for the three case studies without altering the duct geometry. Table 1 presents the details of the experimental case study used in this investigation.

Case Study	**Heated Wall Orientations (Isothermal)**	**Remaining walls Insulated (Adiabatic)**	**Wall surface effect**
CS1	Bottom Heated	Top & side walls	ε = 0.05
CS2	Side Heated	Top, Bottom and side walls	ε = 0.05
CS3	Top Heated	Bottom & Side Walls	ε = 0.05
CS1	Bottom Heated	Top & side walls	ε = 0.85
CS2	Side Heated	Top, Bottom and side walls	ε = 0.85
CS3	Top Heated	Bottom & Side Walls	ε = 0.85

Table 1: Details of the experimental case study used in this investigation

Experiments were conducted at three constant power inputs of 644, 1145, and 1659 W/m², corresponding to Reynolds numbers of 848, 1272, and 1695, respectively, covering the laminar mixed-convection flow regime. Air was drawn over the duct by a blower, and the flow rate was observed with a hot-wire anemometer with an accuracy of 1.6%. Glass wool insulation was used to insulate the test section, which was then covered with aluminium to minimise heat loss to the surroundings. To evaluate the effect of wall surface, the interior surface of the heated plate was tested under two conditions: a polished (mirror-finish) surface with a low emissivity of approximately ε = 0.05, and a surface coated with matte black paint, giving a higher emissivity of approximately ε = 0.85.

To evaluate the heated plate and the adiabatic duct walls, as well as the intake and exit air temperatures, 36 Type-K thermocouples (Chromel–Alumel, accuracy ±1 °C) were implanted. To record the streamwise wall-temperature distribution, thermocouples were positioned lengthwise along the heated plate surface and the adiabatic walls at a consistent spacing of 30 mm. The mean air temperature was calculated by measuring the air temperatures at the entrance and outflow using two thermocouples. Before testing, an ice-water bath was used to calibrate each thermocouple against a precise reference thermometer.

For each case study (CS1, CS2, CS3), the blower was switched on first and adjusted to the flow rate corresponding to the required Reynolds number. After the silicon rubber strip heater,

a variable transformer was used to adjust the input power to the required value. After about three hours, the system reached steady state, as indicated by the wall and outlet air temperatures changing little. The wall temperature and inlet/outlet air temperature readings were then recorded. This procedure was repeated for each case study of Reynolds number, heat flux, and surface condition (polished/black) across all three heating orientations, giving a full test matrix of 3 (orientation) × 3 (Re/Q) × 2 (surface) = 18 experimental runs.

Method of data analysis

To measure the heat-transfer properties under various heating orientations, the experimental data from the horizontal rectangular duct are examined. The effects of convection and radiation heat transfer, Reynolds number (Re), Grashof number (Gr), convective and radiative Nusselt number (Nu) and Total Nusselt numbers are considered. The buoyancy-induced flow structure and, hence, the relative roles of forced and natural convection are expected to be altered by the orientation of the heated wall. The recorded temperatures, airflow rate, and velocity data, along with electrical power input, are used to determine the heat-transfer rate and related dimensionless parameters for each heating orientation: bottom, top, and side heating. The total power supplied to the heater is;

$$Q_t = VI \tag{1}$$

The heat flux from the test section heated area is denoted by [9]:

$$q = \frac{Q_{tot}}{A_s} \tag{2}$$

The expression for the total heat transmission from the channel's heated wall is:

$$Q_t = Q_c + Q_r \tag{3}$$

The hydraulic diameter of the test section is calculated as follows;

$$D_h = \frac{2WH}{W+H} \tag{4}$$

The convective Nusselt number and local convective heat transfer coefficient from the heated wall surface are as follows [9]:

$$h_c = \frac{Q_c}{A_s(T_w - T_b)} \tag{5}$$

The mean temperature of the entering air was measured at the start and finish of the test segment using two thermocouples [1].

Where

$$T_b = (T_{in} + T_{out})/2$$

$$Nu_c = \frac{Q_c D_h}{A_s (T_w - T_b) k} \tag{6}$$

The local radiative heat transfer coefficient with wall factor and convective Nusselt number from the heated wall surface are given as [25];

$$h_r = \varepsilon \sigma F_{h-s} (T_w + T_s)(T_w^2 + T_s^2) \tag{7}$$

$$Q_r = h_r \, A_s (T_w - T_b) \tag{8}$$

$$Nu_r = \frac{Q_r D_h}{A_s (T_w - T_b) k} \tag{9}$$

The combined convection and radiation Nusselt number obtained from Equations 6 and 8 for the heated wall:

$$Nu_t = Nu_c + Nu_r \tag{10}$$

The combined convection and radiation contribution obtained from the following formula gives a

$$\%Q_c = \frac{Q_c}{Q_c + Q_r} X100 \tag{11}$$

$$\%Q_r = \frac{Q_r}{Q_r + Q_c} X100 \tag{12}$$

Uncertainty calculation

Temperature and velocity measurements account for the full uncertainty in the final experimental results. Experimental accuracy often depended on the specific measurement devices used. The Nusselt numbers were evaluated using measurable quantities to approximate their uncertainty. The uncertainty analysis was carried out on all measured data to ensure the precision and dependability of the experiments.

The uncertainty in convective heat transfer is calculated from the following equations;

$$U_{h_c} = h_c \sqrt{\left(\frac{U_{Q_c}}{Q_c}\right)^2 + \left(\frac{U_A}{A}\right)^2 + \left(\frac{U_{\Delta T}}{\Delta T}\right)^2} = \pm 0.011$$

The uncertainty in convective heat transfer is calculated from the following equations;

$$U_{h_r} = \sqrt{\left(\frac{\partial h_r}{\partial \varepsilon} U_\varepsilon\right)^2 + \left(\frac{\partial h_r}{\partial T_\omega} U_{T\,\omega}\right)^2 + \left(\frac{\partial h_r}{\partial T_{sur}} U_{T\,sur}\right)^2} = \pm 0.012$$

The uncertainty in convective Nusselt number is calculated from the following equations;

$$\frac{U_{Nu_c}}{Nu_c} = \sqrt{\left(\frac{U_{h_c}}{h_c}\right)^2 + \left(\frac{U_{D_h}}{D_h}\right)^2 + \left(\frac{U_k}{k}\right)^2} = \pm 0.014$$

The uncertainty in the radiative Nusselt number is calculated from the following equations;

$$\frac{U_{Nu_r}}{Nu_r} = \sqrt{\left(\frac{U_{h_r}}{h_r}\right)^2 + \left(\frac{U_{D_h}}{D_h}\right)^2 + \left(\frac{U_k}{k}\right)^2} = \pm 0.016$$

The overall uncertainty of the total Nusselt number is calculated from the following equations;

$$U_{Nu_{total}} = \sqrt{U_{Nu_c}^2 + U_{Nu_r}^2} = 0.030$$

The temperature uncertainties of the heating wall surface and the other adiabatic walls were determined to be within ±0.05 °C, and an anemometer was used to measure airflow with an accuracy of ±1.6%. It was determined that the total Nusselt number had an absolute uncertainty of ±0.030. The overall uncertainty in the computed Nusselt number for the heated vertical wall of the test section was found to be less than ±3% across all scenarios investigated in this study. All uncertainty estimates were obtained using the procedure outlined in Coleman and Steele [26].

Result and discussion

The thermal and heat-transfer properties of the heated wall in a horizontal duct under mixed-convection and radiation conditions are investigated using the experimental findings presented in this section. The observed heated-wall temperature and the convective and radiative Nusselt numbers are used to assess the effects of the operational parameters: Reynolds number, heat flux, surface emissivity, and heating configuration. To determine the impact of heated-wall orientation on the interplay between forced convection, buoyancy-driven flow, and thermal radiation, three heating configurations (CS1, CS2, and CS3) are examined. To evaluate the thermal development and heat-transfer behaviour within the test section, the data are analysed. In the result and discussion, the impact of Reynolds number and heat flux on the heated-wall temperature is first examined, and then the impact of surface emissivity is evaluated. The radiative Nusselt values are then compared to determine the relative contributions of convection and radiation to the overall heat transfer.

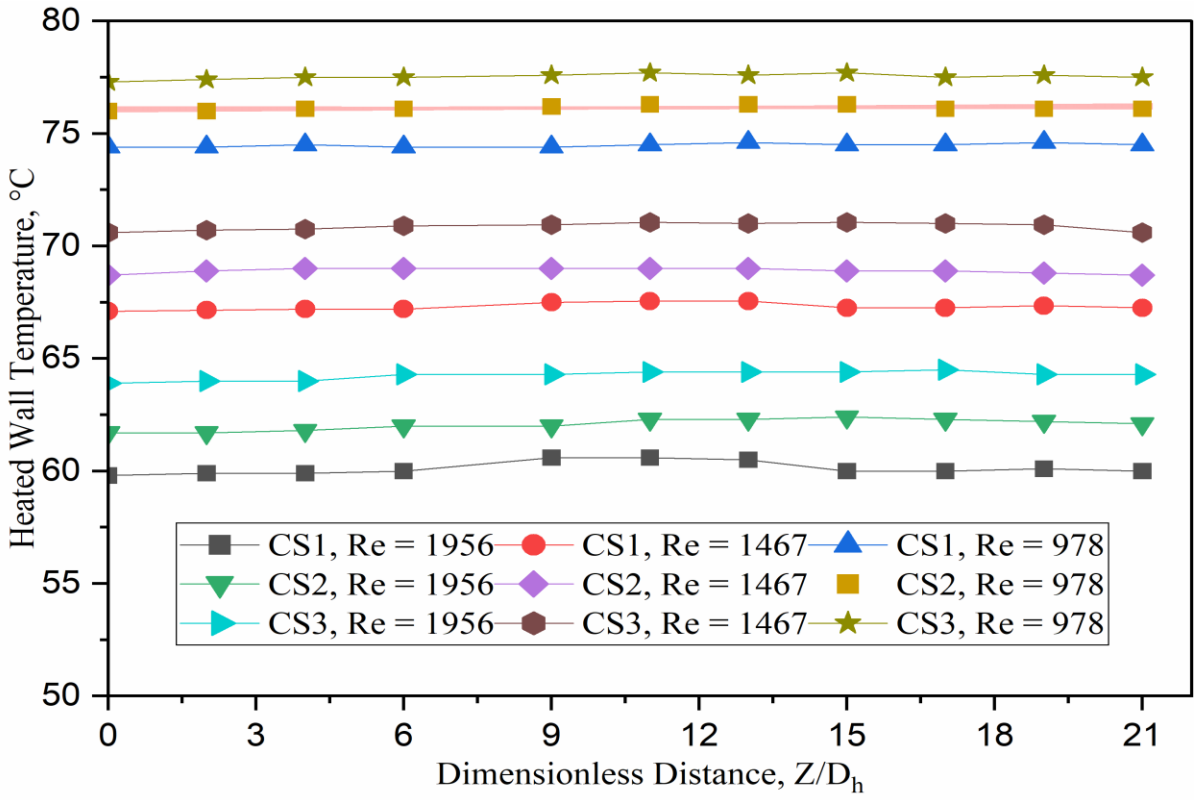


Fig. 4 Effect of the heated wall temperature distribution at different Reynolds numbers (q = 1659 W/m^2, ε = 0.05)

Distribution of heated wall surface temperature

Figure 4 shows the temperature variation of the heated wall along the dimensionless axial distance of the test section for three heating configurations of bottom, side, and top with three Reynolds numbers. Across all three configurations, the Reynolds number increases, and the heated wall surface temperature decreases significantly. This behaviour is attributed to the increased forced-convection heat-transfer coefficient at higher Reynolds numbers, which enhances heat removal from the heated wall. Under a constant heat flux of 1659 W/m², there is a definite relationship between the heating setup and the hot-wall temperature. The average wall temperatures for CS1, CS2, and CS3 for Re = 1956 are around 60.0°C, 61.8°C, and 63.9°C, respectively for polished surface. As a result, compared to CS1, CS2 and CS3 show temperature increases of around 3.0% and 6.5%, respectively. These variations decrease to around 2.23% and 5.21% at Re = 1467, and to 2.29% and 4.17% at Re = 978, respectively. This indicates that the orientation of the heated wall strongly influences the interaction between forced and buoyancy-driven flow and the axial wall temperature. There are very few differences in the axial wall temperature distribution throughout the duct. The thermally growing zone shows a modest temperature increase, followed by a nearly steady or slightly declining trend downstream. The emissivity is very low, so the radiative part is very small and the convective part is large.

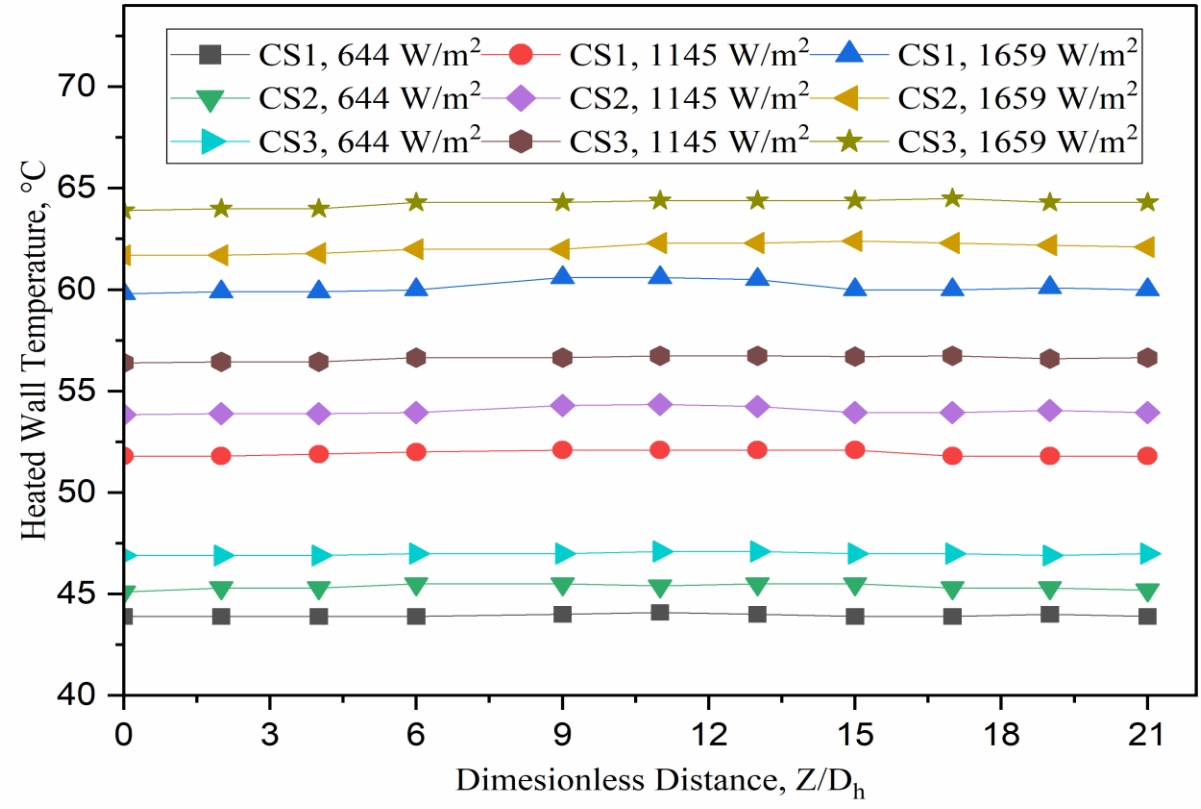


Fig 5 Effect of the heated wall temperature distribution at different heat flux (Re = 1956, ε = 0.05)

Figure 5 shows the temperature variation of the heated wall along the dimensionless distance for three heat fluxes and the three heating configurations. The findings show that for all three case studies, the heated-wall temperature rises steadily as heat input increases. The hot-wall temperature gradually rises as heat input increases. Across all heat inputs, the wall temperature is lowest in CS1, then in CS2 and CS3. Compared with CS1, CS2 and CS3 exhibit temperature increases of around 3.9% and 7.1% at 644 W/m², respectively. The resulting disparities rise to 3.9% and 8.9% at 1145 W/m², and to around 3.2% and 6.9% at 1659 W/m², respectively. Among the three layouts, CS1 offers the most efficient heat transfer, whereas CS3 has higher wall temperatures, suggesting a somewhat worse capacity to remove heat. The results also show that, especially at 1145 W/m², the impact of heating design becomes increasingly noticeable as the applied heat input increases. Altering the buoyancy-induced flow and thermal boundary-layer growth shows that the heating direction substantially impacts heat-transfer performance.

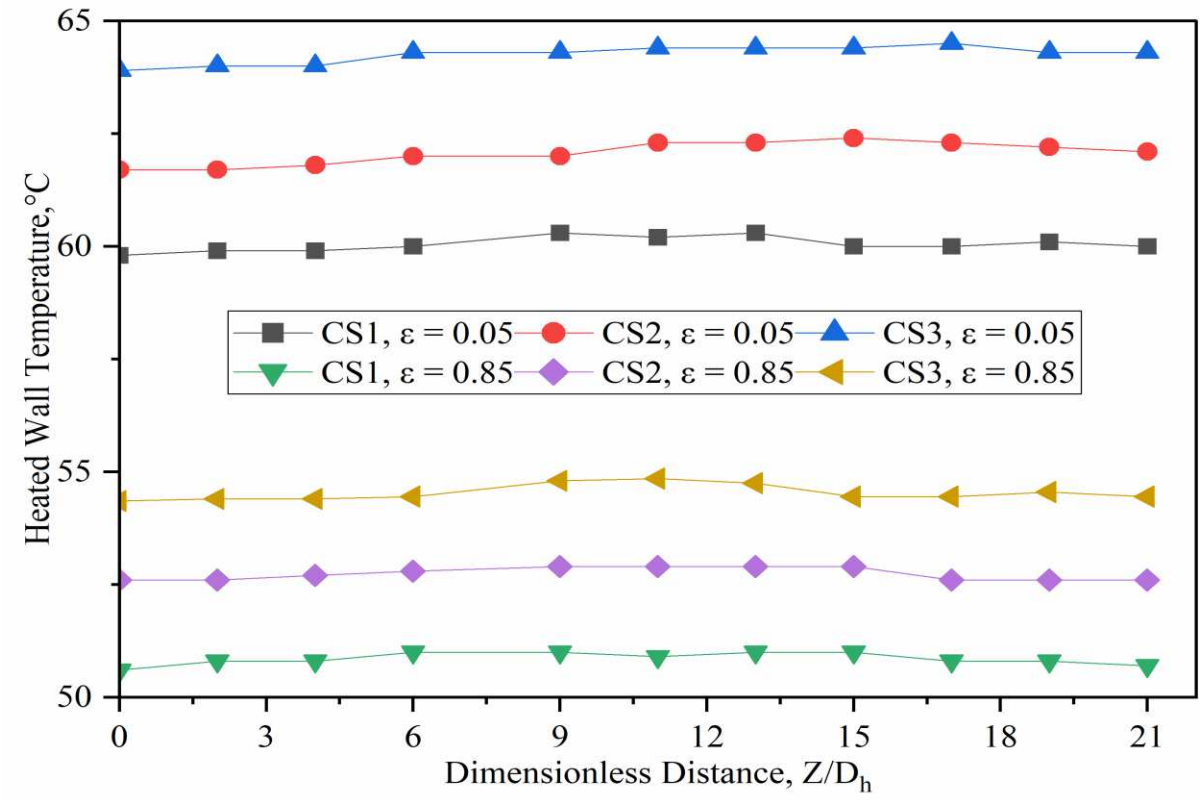


Fig 6 Effect of the heated wall temperature distribution
(Re = 1956, q = 1659 W/m^2)

The heated wall temperature in Figure 6 shows a relatively consistent distribution over the dimensionless distance at Re = 1956 and a constant heat flux of 1659 W/m². CS3 has the highest average wall temperature, 64.25 °C, when ε = 0.05, followed by CS2 at 62.20 °C and CS1 at 60.35 °C. When the emissivity is increased to 0.85, the wall temperature decreases significantly to approximately 54.5 °C for CS3, 52.7 °C for CS2, and 50.8 °C for CS1. This corresponds to temperature reductions of approximately 15.2% for CS3, 15.3% for CS2, and 15.8% for CS1, respectively. The reduction in wall temperature is attributed to enhanced radiative heat loss due to higher surface emissivity. For both emissivity conditions, CS1 maintains the lowest wall temperature, whereas CS3 records the highest temperature, indicating that the heating configuration significantly influences the thermal behaviour of the heated wall. Increasing emissivity from 0.05 to 0.85 reduces the heated wall temperature by approximately 15.8%, with the maximum reduction observed for CS1.

Effect of Convection on Heat Transfer Characteristics

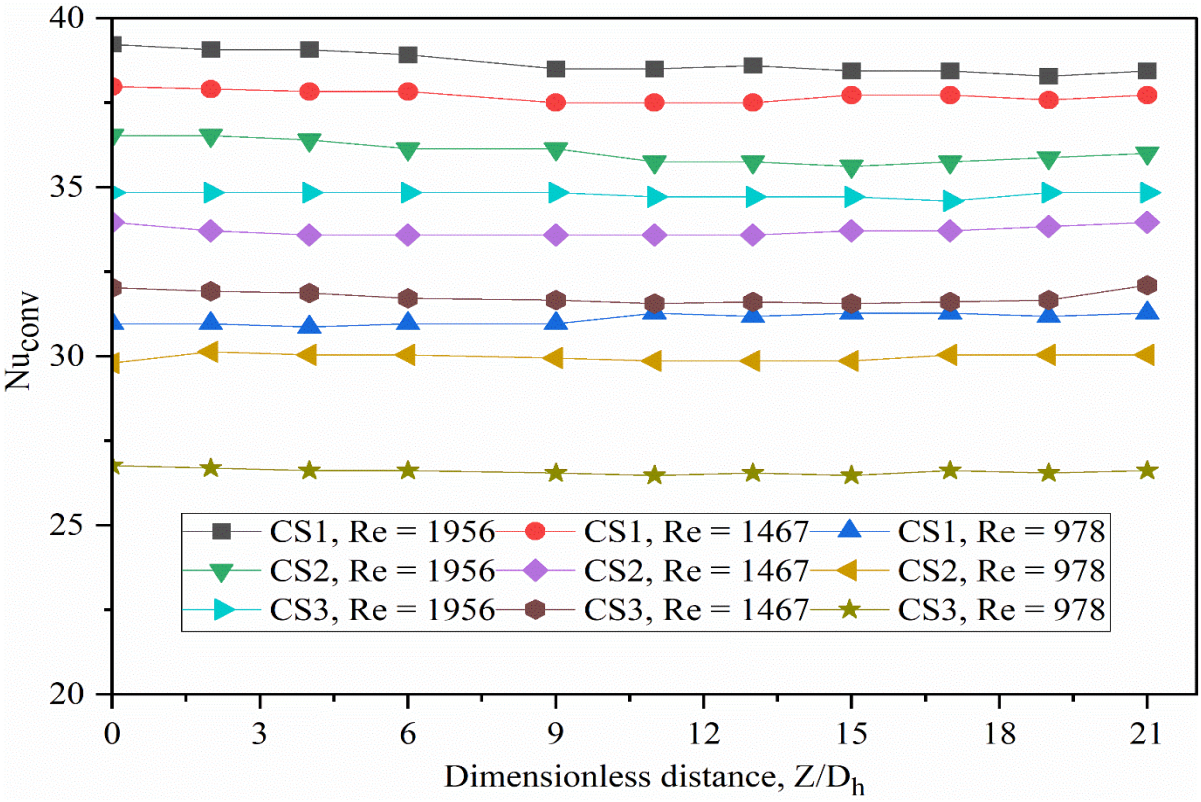


Fig 7 Distribution of convective Nusselt number along the heated wall
(q = 1659 W/m2, ε = 0.05)

Figure 7 shows the distribution of the convective Nusselt number on the heated wall. The convective Nusselt number varies slightly in the developing region but stays reasonably constant over the dimensionless distance at q = 1659 W/m² and ε = 0.05. Average convective heat transfer is greatly improved by raising the Reynolds number from 848 to 1272 and 1695. The Nusselt numbers for CS1, CS2, and CS3 are approximately 39, 36.5, and 34.8 at Re = 1695, respectively. The equivalent values are about 38, 33.7, and 31.8 at Re = 1272 and 31, 30, and 26.5 at Re = 848. Compared with increasing the Reynolds number to 1695, which enhances the convective Nusselt number by approximately 25.8% for CS1, 21.7% for CS2, and 31.3% for CS3. Similarly, increasing (Re) from 848 to 1272 results in improvements of approximately 22.6%, 12.3%, and 20.0% for CS1, CS2, and CS3, respectively. When (Re) increases from 1272 to 1695, the corresponding enhancements are approximately 2.6%, 8.3%, and 9.4%. These results confirm that increasing the Reynolds number strengthens forced convection, thereby enhancing the convective Nusselt number. Among the three heating configurations, CS1 consistently exhibits the highest convective heat-transfer performance, whereas CS3 records the lowest values under all Reynolds-number conditions. As a result, stronger forced convection and higher Nusselt numbers are encouraged by increasing Reynolds numbers, with CS1 continuously offering the best convective heat-transfer performance.

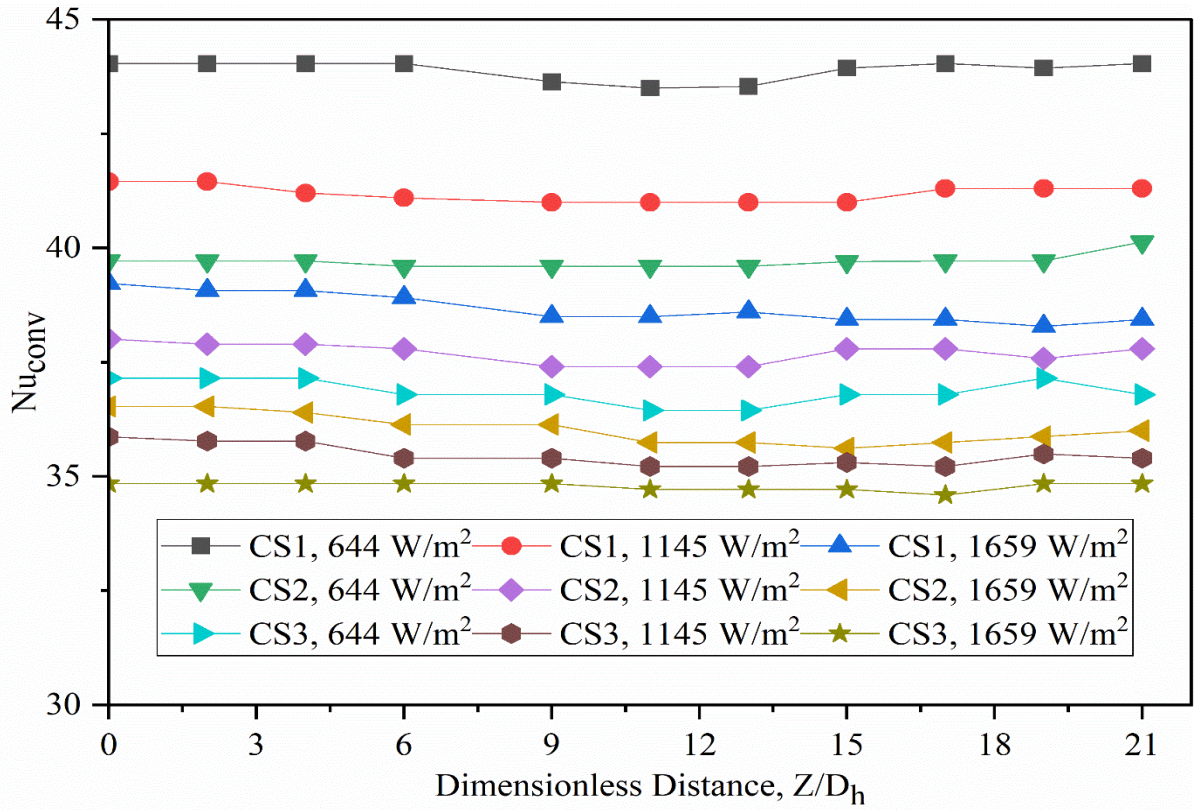


Fig 8 Distribution of Convective Nusselt number along the heated wall
(Re = 1956, ε = 0.05)

The distribution of convective Nusselt number for Reynolds number 1696 and polished surface (ε = 0.05) is seen in Figure 8. The convective Nusselt number generally decreases across all three case studies as the heat input increases from 644 to 1659 W/m². Stronger convective heat transfer is observed in CS1, which has the highest values, followed by CS2 and CS3. The Convective average Nusselt number reduces by 12.3%, from around 43.9 at 644 W/m² to 38.5 at 1659 W/m². Similarly, CS2 drops from around 39.6 to 36.0, a 9.1% decline, while CS3 drops from roughly 36.7 to 34.8, a 5.2% decline. Overall, the findings show that, depending on the arrangement, increasing heat input reduces Nusselt convection by approximately 5–13%. The rise in wall temperature, which reduces the relative convective heat-transfer driving force, is responsible for the drop in convective Nusselt number with increasing heat input. Because of its more advantageous heating configuration and stronger buoyancy-airflow interaction, CS1 has a higher Nusselt number.

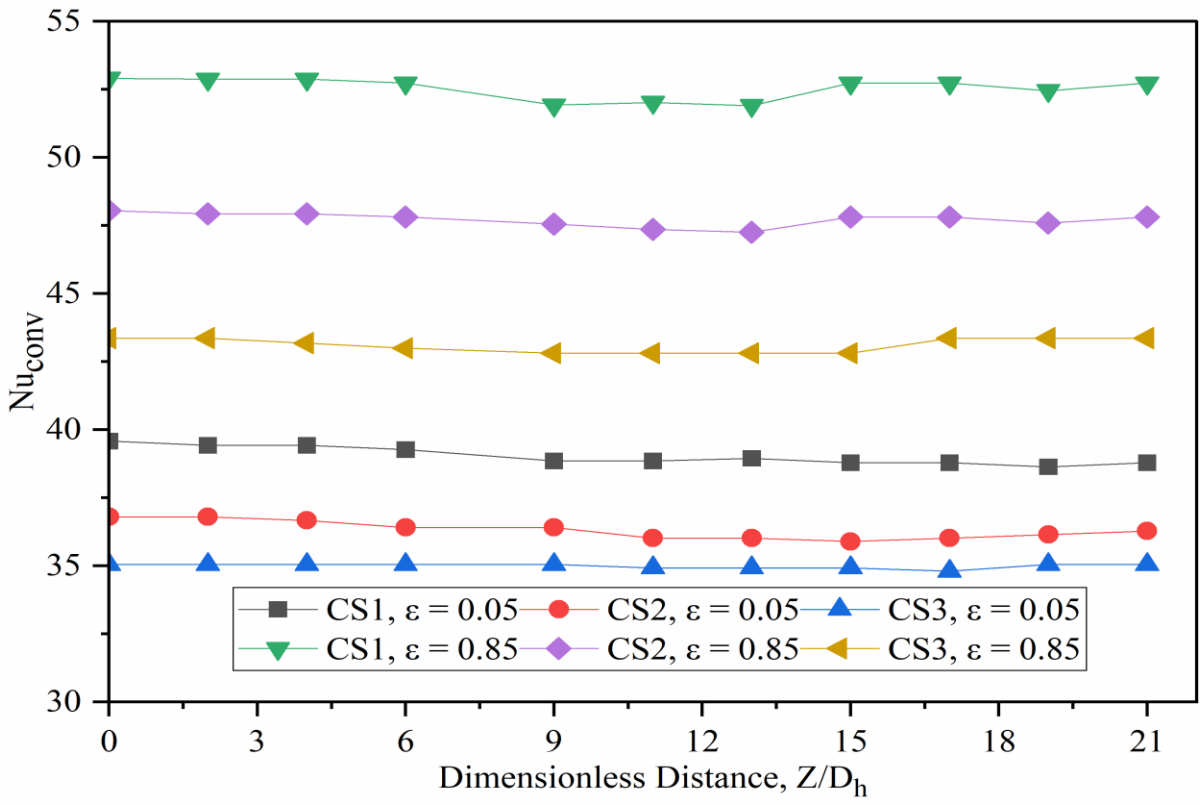


Fig 9 Comparison of convective Nusselt number along the heated wall
(q = 1659 W/m2, Re = 1956)

Figure 9 clearly demonstrates how surface emissivity affects the convective Nusselt number for three case studies. The rate of Nusselt convective for polished surfaces (ε = 0.05) is approximately 39, 37, and 35.5 for CS1, CS2, and CS3, respectively. Similarly, the Nusselt convective values for black surfaces (ε = 0.85) are approximately 52.5, 47.5, and 43.35 for CS1, CS2, and CS3, respectively. As emissivity increases from 0.05 to 0.85, the convective Nusselt numbers for CS1, CS2, and CS3 increase from 39.0 to 52.5, 37.0 to 47.5, and 35.5 to 43.0, corresponding to enhancements of 34.6%, 28.4%, and 21.1%, respectively. Overall, increasing emissivity from 0.05 to 0.85 increases Nusselt convection rate by around 21–35%, indicating that surface radiation plays a major role in heat-transfer efficiency. Compared to polished (ε = 0.05), the greater emissivity surface (ε = 0.85) emits substantially more heat radiation. The total heat transfer from the heated wall to the surroundings is improved by enhanced radiative heat dissipation, which lowers the wall temperature. As a result, the temperature differential between the bulk air and the heated wall widens, enhancing convective heat transfer and raising the convective Nusselt number.

Effect of Wall Surface Emissivity on Heat Transfer Characteristics

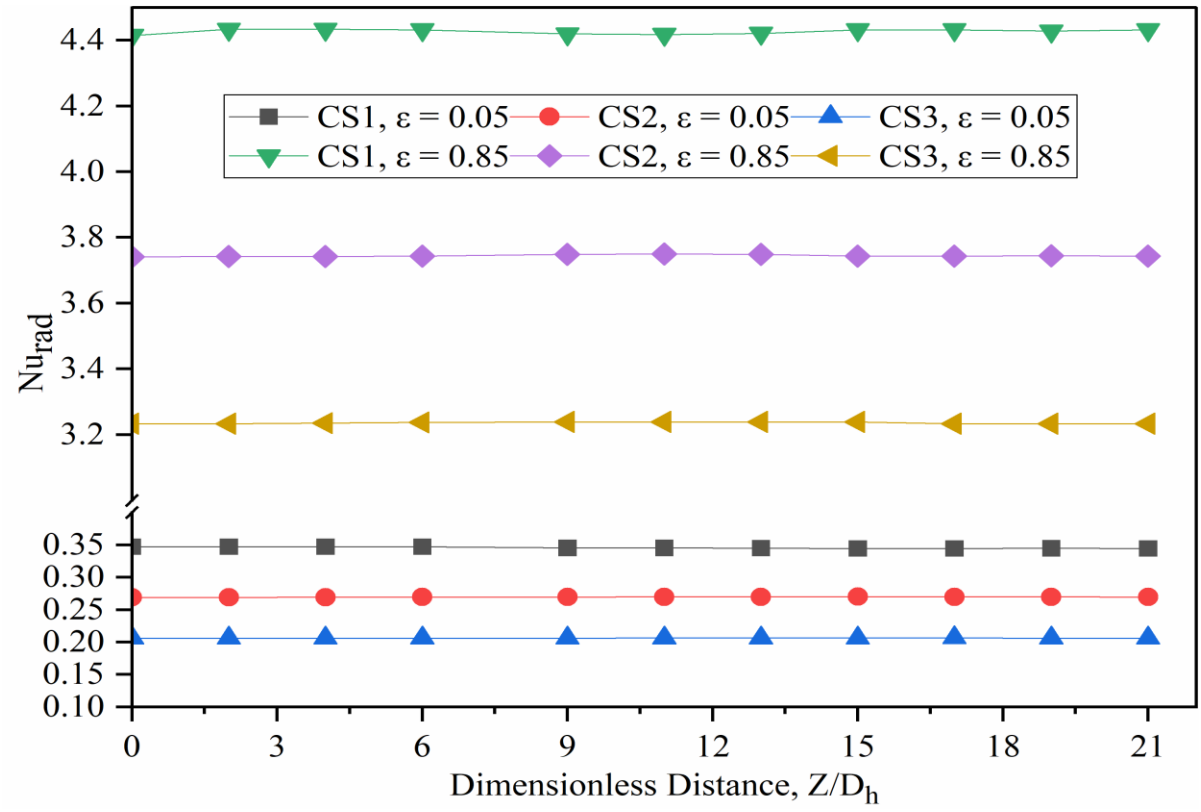


Fig 10 Comparison of the radiative Nusselt number along the heated wall
(q = 1659 W/m2, Re = 1956)

Figure 10 shows the radiative Nusselt number as a function of the dimensionless distance for CS1, CS2, and CS3 at ε = 0.05 and 0.85. The results illustrate that radiative heat transfer is strongly affected by a surface's heat emission. At a value of ε equal to 0.05, the average radiative values are about 0.35 for CS1, 0.26 for CS2, and 0.20 for CS3. When the emissivity is raised to 0.85, these values go up to about 4.41, 3.75, and 3.23. As a result, the improvements are about 11.60%, 13.42%, and 15.15% for CS1, CS2, and CS3, respectively. CS3 shows the largest relative increase because of its lower beginning radiative contribution, even if CS1 offers the highest absolute radiative heat-transfer rate. The configurations consistently follow the sequence CS1 > CS2 and CS2 > CS3 for a given emissivity. At ε=0.05, CS2 and CS3 have radiative Nusselt values that are approximately 25.7% and 42.9% lower than those of CS1. Additionally, the highly uniform profiles along the dimensionless distance indicate that the radiative heat-transfer influence is nearly constant across the channel. The results clearly indicate that increasing emissivity is the most effective way to enhance radiative heat transfer efficiency.

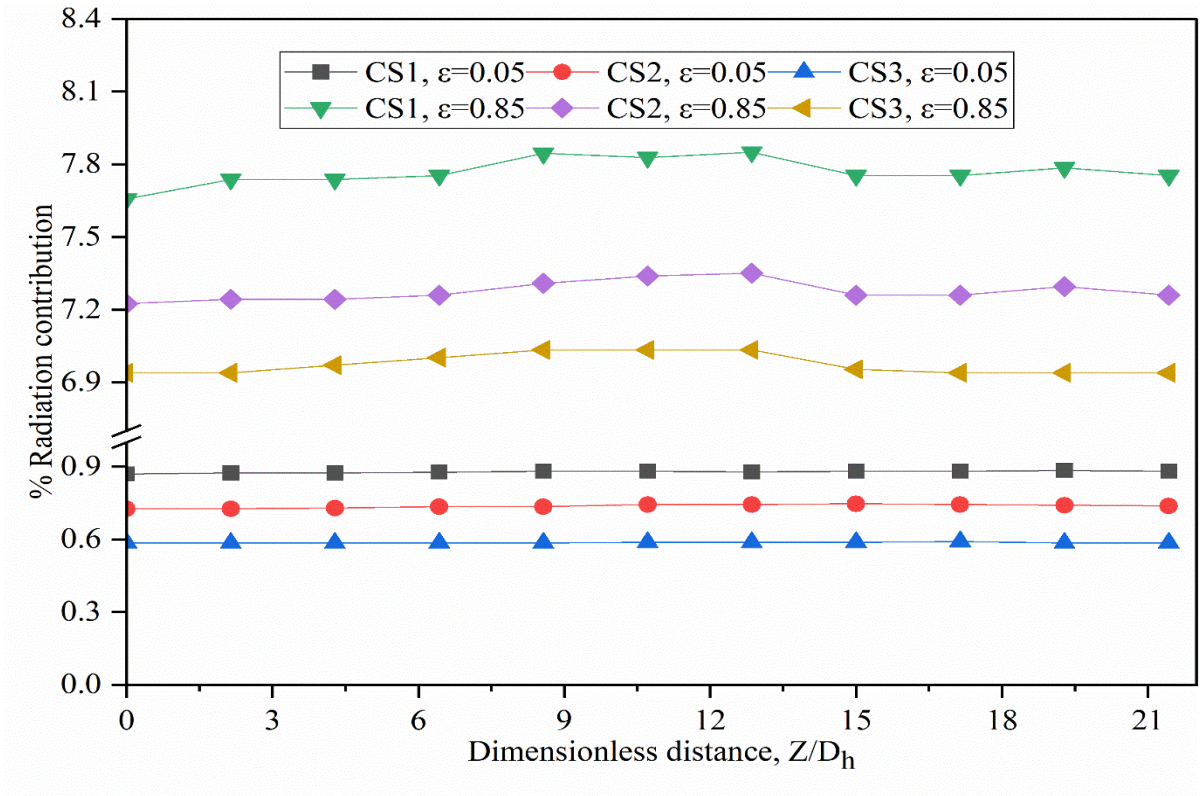


Fig 11 Comparison of the percentage radiation contribution along the heated wall ($q = 1659$ W/m^2, Re = 1956)

For cases with a Reynolds number of 1695, the contribution of radiation varies along the entire dimensionless distance, as shown in Figure 11. It has been found that surface emissivity influences the radiative contribution. The radiation contributions for the CS1, CS2, and CS3 polished surfaces are approximately 0.86, 0.72, and 0.58, respectively. For a black surface, the radiation contributions are approximately 7.65, 7.29, and 6.99, respectively. In this case CS1, CS2, and CS3, there is an improvement of around 7.90%, 9.13%, and 11.05%, respectively. The contributions of radiation from CS2 and CS3 are about 16.3% and 32.6% lower than those of CS1 at $\varepsilon = 0.05$, respectively. The differences are reduced to about 4.7% and 8.6% at $\varepsilon = 0.85$, implying that the relative performance of the designs improves at higher emissivity values. For very small differences in the intermediate and downstream regions, the contribution of radiation is quite consistent throughout the dimensionless distance. Generally, the results indicate that the key determinant of radiation contribution is emissivity rather than configuration. The major finding is that the radiation share increases substantially across all three configurations as the emissivity increases from 0.05 to 0.85. Moreover, the curves exhibit fairly uniform behaviour within the channel, indicating that the influence of axial position on the radiation share is minimal.

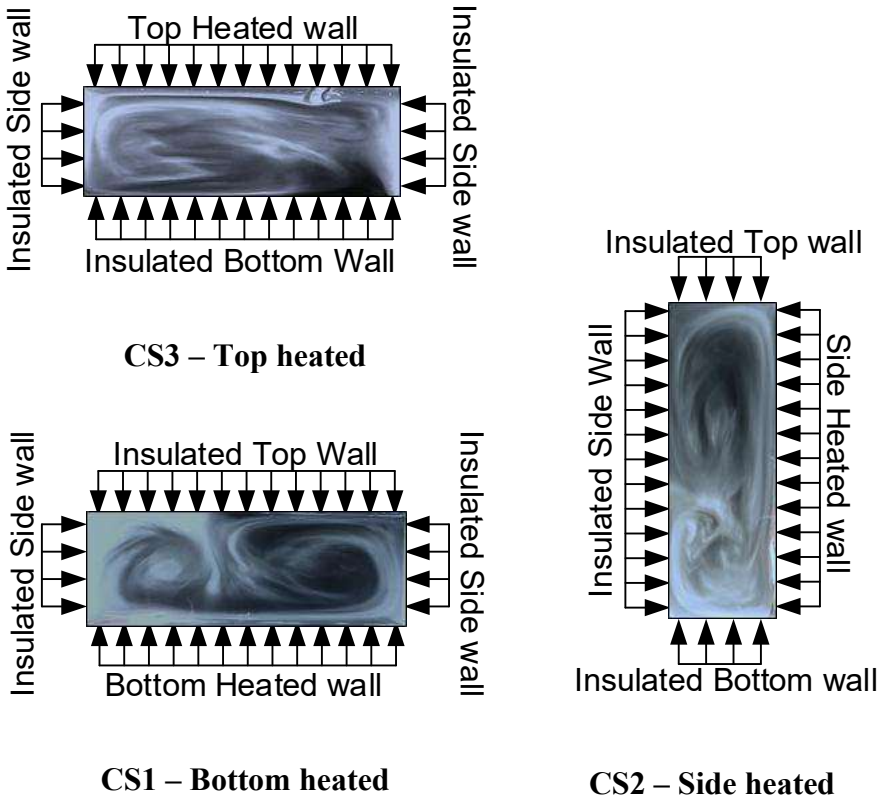


Fig. 12 Schematic representation of the heating configurations with flow structure

Figure 12 illustrates the mixed-convection flow characteristics for three distinct heating orientations: bottom (CS1), top (CS2), and side (CS3). In CS1, the bottom-heated wall induces buoyancy-driven upward flow. Cooler fluid, however, falls near the insulated upper wall. Inside the horizontal channel, two noticeable counter-rotating recirculation cells form. Under applied heating conditions, these vortices improve fluid mixing, redistribute thermal energy, and significantly impact mixed-convection heat-transfer performance across the test area. In CS2, the heated sidewall induces buoyancy-driven upward flow along the heated surface, and cooler fluid flows downhill near the opposing insulated wall. Different recirculating vortices are created in the channel as a result of this interaction. Under mixed-convection conditions, the resulting flow circulation affects local heat-transfer properties, enhances thermal transport, and promotes fluid mixing. In CS3, buoyancy prevents vertical motion because heating from above creates a stable stratified hollow with insulated bottom and side walls. Instead of structured cells, the interior exhibits lengthy, horizontally oriented striations, suggesting weak, slow recirculation restricted to the top part. Heat transport is dominated by conduction, as evidenced by the small clockwise eddy near the heated wall and the relatively quiet bottom core.

Effect of Combined Convective and Radiative Heat Transfer Characteristics

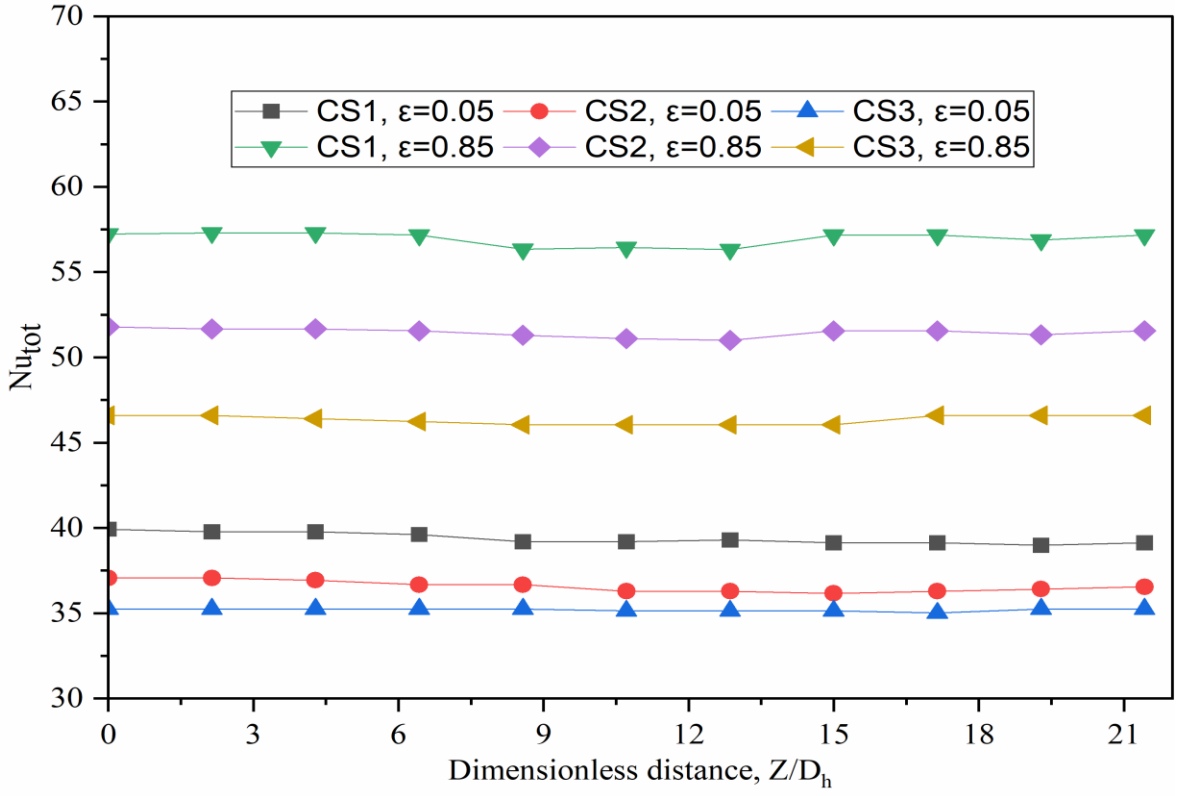


Fig 13 Comparison of the total Nusselt number on the heated wall
(q = 1659 W/m2, Re = 1956)

Figure 13 illustrates the total Nusselt number along the heated wall of the test section. The wall Surface emissivity plays a significant part in increasing heat transfer in each design. In CS1, the total Nusselt number increases from 39.2 to 56.7, representing an increase of about 44.6% for both wall surface emissivity. Similarly, in CS2, it increases from 36.5 to 51.5, a 41.1% increase, and in CS3, it increases from 35.2 to 46.2, a 31.3% increase. CS1 has the most efficient heat transfer irrespective of surface emissivity, followed by CS2 and CS3. There is a slight reduction in the central zone and a slight increment in the downstream zone. The variation along the axial direction in total Nusselt number is minimal. This indicates that the efficient heat-transfer characteristics are retained throughout the entire channel. The results illustrate that heat transfer improves as ε increases, with CS1 showing the greatest sensitivity and the largest increase.

Conclusion

The following findings are obtained from an experimental study of mixed convection and radiation heat transfer in a horizontal rectangular duct with various heating orientations. From the experimental study, it is clear that the heat transfer characteristics of the heated wall are significantly dependent on the heating mechanism, Reynolds number, heat flux, and surface emissivity. With increasing Reynolds number, the performance of forced convection and wall

temperature decreases, and the CS1 black surface yields the highest convective Nusselt number (52.5) and the lowest wall temperature, followed by CS2 and CS3.

As a result of the reduced driving force from the wall-to-air temperature difference, the wall temperature decreases with increasing heat flux. Conversely, an increase in emissivity from 0.05 to 0.85 improves radiative heat transfer, lowering the wall temperature by 15–16% and the convective Nusselt number by 21–35%. For CS1, CS2, and CS3, the total Nusselt number rises by 44.6%, 41.1%, and 31.3%, respectively. Radiation thus plays a crucial role in heat transmission. Since the heat transfer characteristics exhibit a relatively constant axial distribution throughout the experiment, they remain nearly constant.

Overall, the experimental results demonstrate that while increasing Reynolds number encourages convective heat removal, increasing surface emissivity enhances radiative heat transfer and decreases the heated-wall temperature. Among the configurations being studied, CS1 has the highest overall heat-transfer performance, indicating its potential for improved thermal management applications utilising combined convection and radiation.

Acknowledgements
This research was granted by the TRR research scheme (SASTRA-TRR-SOME-2-12022024), SASTRA Deemed University, Thanjavur, Tamil Nadu, India.

Declarations
Conflict of interest: The author declares no conflict of interest from this submission.

References

1. Salman YK, Jalil JM, Khudheyer AF. Experimental Study of Mixed Convection Heat Transfer to Thermally Developing Air Flow in a Horizontal Rectangular Duct. Int. J. Comput. Appl. 2021;174(25):44–53. DOI:10.5120/IJCA2021921172.
2. Maithani R, Silori A, Rana J, Chamoli S. Numerical analysis of heat transfer and fluid flow of wavy delta winglets in a rectangular duct. Therm. Sci. Eng. Prog. 2017;2:15–25. https://doi.org/10.1016/j.tsep.2017.04.002.
3. Dakhil SF, Najim AQ, Abood FA. Experimental enhancement of mixed convection heat transfer in a hot base rectangular channel. J. Phys. Conf. Ser. 2021;1773(1):012026. https://doi.org/10.1088/1742-6596/1773/1/012026.
4. Zhou L, Liu J, Huang Q, et al. Analysis of combined natural convection and radiation heat transfer in a partitioned rectangular enclosure with semitransparent walls. Trans. Tianjin Univ. 2019;25:472–487. https://doi.org/10.1007/s12209-019-00208-9.
5. Rajamohan G, Kumar P, Prakash D, Manimaran R. Effect of differentially heated square channel wall surface radiation on combined convection heat transfer. Heat Transf. Eng. 2025;46(4–5):362–373.https://doi.org/10.1080/01457632.2024.2317608.
6. Rajamohan G, Ramesh N, Kumar P. Mixed convection and radiation studies on thermally developing laminar flow in a horizontal square channel with variable side heated wall. Int. J. Therm. Sci. 2019;140:298–307. https://doi.org/10.1016/j.ijthermalsci.2019.03.002.

7. Rajamohan G, Sung AN, Kumar P, Onn SYH, Manimaran R. Numerical investigation of combined convection and radiation heat transfer in the horizontal ducts heated from different orientations. AIP Conf. Proc. 2022;2676(1):050005. https://doi.org/10.1063/5.0116554.
8. Elatar A, Siddiqui K. The effect of mixed convection on the structure of channel flow at low Reynolds numbers. Int. J. Heat Fluid Flow. 2014;46:29–42. https://doi.org/10.1016/j.ijheatfluidflow.2013.12.005.
9. Tian C, Wang J, Cao X, Yan C, Ala AA. Experimental study on mixed convection in an asymmetrically heated, inclined, narrow, rectangular channel. Int. J. Heat Mass Transfer. 2018;116:1074–1084. https://doi.org/10.1016/j.ijheatmasstransfer.2017.09.099.
10. Rashevski M, Slavtchev S. Natural and mixed convection in a vertical rectangular duct under solar radiation. Theor. Comput. Fluid Dyn. 2026;40:4. https://doi.org/10.1007/s00162-025-00774-w.
11. Serrano D, Sánchez-Delgado S, Pérez-Álvarez R, Acosta-Iborra A. Experimental determination of the convection heat transfer coefficient in an eccentric annular duct. Exp. Therm. Fluid Sci. 2022;136:110664. https://doi.org/10.1016/j.expthermflusci.2022.110664.
12. Mandev E, Manay E. Effects of surface roughness in multiple microchannels on mixed convective heat transfer. Appl. Therm. Eng. 2022;217:119102. https://doi.org/10.1016/j.applthermaleng.2022.119102.
13. Liu B, Liu Z, Xi Y, et al. Study on the effects of non-uniform structures on enhanced heat transfer and flow performance. J. Therm. Anal. Calorim. 2026;151:5527–5570. https://doi.org/10.1007/s10973-025-15263-9.
14. Long J, Yang BW, Wu T, Zhang B. Numerical investigation of turbulent mixed convection flow and heat transfer characteristics of 2 × 2 subchannels with spacer grids. Energy Sci. Eng. 2023;11(3):1160–1176. https://doi.org/10.1002/ese3.1386.
15. Ajmera SK, Mathur AN. Experimental investigation of mixed convection in a multiple-ventilated enclosure with discrete heat sources. Exp. Therm. Fluid Sci. 2015;68:402–411. https://doi.org/10.1016/j.expthermflusci.2015.05.012.
16. Muralikrishna Y, Rao CG. Parametric and comparative studies on fluid flow and heat transfer from uniformly and non-uniformly heated plates. J. Therm. Anal. Calorim. 2024;149:1761–1775. https://doi.org/10.1007/s10973-023-12730-z.
17. Das D, Roy M, Basak T. Studies on natural convection within enclosures of various (non-square) shapes – A review. Int. J. Heat Mass Transfer. 2017;106:356–406. https://doi.org/10.1016/j.ijheatmasstransfer.2016.08.034.
18. Birinci S, Saglam M, Sarper B, Aydin O. Effect of heaters' clearance on mixed convection cooling performance in a discretely heated horizontal duct. Int. J. Therm. Sci. 2021;163:106859. https://doi.org/10.1016/j.ijthermalsci.2021.106859.
19. Hidki R, El Moutaouakil L, Boukendil M, Charqui Z, Zrikem Z, Abdelbaki A. Numerical analysis of mixed convection coupled with thermal radiation in a ventilated channel containing various heat-generating blocks. In: Advances in Applied Mechanics.

Lecture Notes in Mechanical Engineering. Springer, Cham; 2024:87–98. https://doi.org/10.1007/978-3-031-49727-8_8.
20. Amran MF, Sultan SM, Tso CP. A comprehensive review of mixed convective heat transfer in tubes and ducts: Effects of Prandtl number, geometry, and orientation. Processes. 2024;12:2749. https://doi.org/10.3390/pr12122749.
21. Noori S, Sheidani A, Kamari D. Mixed convection and radiation heat transfer in an enclosure filled with unevenly heated plates at different configurations. J. Therm. Anal. Calorim. 2023. https://doi.org/10.22034/jast.2023.357234.1127.
22. Karabulut K, Alnak Y. Mixed convection heat transfer enhancement and flow structure research in vertical channels having different numbers of warmed obstacle series with Al2O3-water nanofluid. Heat Mass Transfer. 2026;62(5):52. https://doi.org/10.1007/s00231-026-03682-9.
23. Sushma S, Chandrashekar TK. An experimental investigation on performance of heat transfer using heat sink of different shape for electronic applications. Indian J. Sci. Technol. 2021;14(35):2789–2801. https://doi.org/10.17485/IJST/v14i35.1179.
24. Abedallh AS, Alomar OR, Yasin NJ. Numerical and experimental investigation on mixed convection heat transfer inside cavity heated from below with reciprocating moving upper surface. Int. Commun. Heat Mass Transfer. 2024;159(Part C):108242. https://doi.org/10.1016/j.icheatmasstransfer.2024.108242.
25. Prakash M, Singh SN. Experimental and numerical study of mixed convection with surface radiation heat transfer in an air-filled ventilated cavity. Int. J. Therm. Sci. 2022;171:107169. https://doi.org/10.1016/j.ijthermalsci.2021.107169.
26. Coleman HW, Steele JWG. Experimentation and uncertainty analysis for engineers. 4th ed. New York: Wiley, 2018.